Chaos in Solitary VCSELs: Exploring the Parameter Space With Advanced Sampling

Virte, Martin; Ferranti, Francesco

Published in:
Journal of Lightwave Technology

DOI:
10.1109/JLT.2017.2784847

Publication date:
2018

License:
Unspecified

Document Version:
Accepted author manuscript

Chaos in solitary VCSELs: Exploring the parameter space with advanced sampling

Martin Virte, *Member, IEEE,* Francesco Ferranti, *Senior Member, IEEE*

***Abstract*—We explore the parameter space of the so-called spin-flip model by advanced sampling techniques to analyze the requirements leading to polarization chaos in solitary Vertical-Cavity Surface-Emitting Lasers (VCSELs). We first investigate the performances of different sampling techniques for multi-dimensional parameter space exploration. Purely random sampling and tensor-product grids require a large amount of samples to uniformly cover the whole space, and we show that other schemes are highly superior to this regards, hence allowing a reduced number of samples and computation to be used to reach the same level of insight in the system behaviour. Considering the scarcity of the chaotic regions and their sharp boundaries, combined with quite involved computations to identify chaotic dynamics, the proposed approach is shown to be highly beneficial. Here, we are able to highlight two thresholds limiting the range of injection current for which chaos can be observed, and to link them to a fine balance between the spin relaxation rate and the birefringence.**

***Index Terms*—Semiconductor Laser, VCSEL, chaos, optical chaos, parameter space exploration, sampling schemes.**

I. Introduction

NUMERICAL modelling is the keystone of system optimization. A good model can be used to optimize the system parameters to reach a certain level of performances or to find the most robust configuration for a given application. Numerical modelling has become more and more complex, hence requiring significant amount of computing power and time. Simultaneously, the number of system parameters has also seen a substantial increase, and it has now become a real challenge to efficiently explore those highly multidimensional parameter spaces. Using a number of linearly spaced values for each parameter in an N-D parameter space, and then forming the full grid by taking all possible combinations of the different parameter values leads to a quite large number of samples: for a system with 6 parameters, taking 10 different values for each parameter leads to 10^6 samples. On the other hand, a random sampling can be more efficient, but its intrinsic randomness cannot guarantee that the samples will uniformly cover the whole parameter space. To overcome this difficulty, advanced sampling techniques are a promising alternative combining a good distribution of samples and a reduced number of points, hence much less simulations and computations. Among advanced sampling methods for computer experiments, the Latin hypercube sampling (LHS) [1] and quasi-random sequences (also called "low discrepancy sequences"), such as Halton and Sobol sequences, are widely used solutions [2], [3].

The issue of parameter space exploration is particularly acute in the field of nonlinear dynamics and chaotic systems where extremely sudden dynamical changes can appear, hence forming ragged chaotic regions. Such cases are therefore the most challenging situations which typically requires a dense sampling grids to precisely identify the set of parameters corresponding to chaotic dynamics. Nowadays, the computation of 2-D grids (maps) remains a standard exploration techniques in the field [4]–[6]. As previously mentioned, extending this grid approach to N-D parameter spaces is very inefficient. Advanced sampling techniques can therefore represent a significant boost of efficiency in this field. Here, as a test-bed, we look into polarization chaos dynamics generated by solitary laser diodes [7]. Even though an excellent qualitative agreement has been obtained between numerical and experimental results, the conditions bringing up polarization chaos in Vertical-Cavity Surface-Emitting Lasers (VCSELs) remain quite unclear especially as it has only been observed, so far, in peculiar structures using quantum dot as gain medium [8] and in strained VCSELs [9]. Parameter space exploration can therefore provide a substantial insight to determine which parameters are the most critical and in which range chaos is most likely to be found. To investigate the polarization dynamics of VCSELs, we use the well-known Spin-Flip Model (SFM) [10], [11] which takes into account the competition between polarization modes and accurately reproduces the chaotic dynamics that has been observed experimentally [7].

In this work, we tackle the following two aspects. We first evaluate the performances of different sampling schemes adapted to generate a set of values for the parameters of the VCSEL model. Second, we apply the best sampling scheme (best with respect to a figure of merit called discrepancy measure) to investigate the problem of chaotic free-running VCSELs. We unveil essential conditions for the emergence of chaotic dynamics, and thus validate the suggested approach based on advanced sampling techniques. We are able to highlight two thresholds limiting the range of injection current for which chaos can be observed, and to link them to a fine balance between the spin relaxation rate and the birefringence.

Manuscript received August 1st, 2017. Accepted December 14th, 2017.

This work has been supported by the Research Foundation - Flanders (FWO), the METHUSALEM program of the Flemish Governments and the Interuniversity Attraction Pole Program (IAP P7-35 photonics@be) of the Belgian Science Policy Office (Belspo).

Martin Virte is with Brussels Photonics (B-PHOT), Vrije Universiteit Brussel, Pleinlaan 2, 1050 Brussel, Belgium. He is a post-doctoral Fellow from the Research Foundation - Flanders (FWO). Email: mvirte@b-phot.org

F. Ferranti is with the Microwave Department, Institut Mines-Télécom (IMT) Atlantique, CNRS UMR 6285 Lab-STICC, 29238 Brest CEDEX 3, France. Email: francesco.ferranti@imt-atlantique.fr

TABLE I
QUADRATIC DISCREPANCY ESTIMATIONS. ALL VALUES HAVE BEEN MULTIPLIED BY 10^4 TO IMPROVE THE READABILITY.

number of samples	**50**	**100**	**300**
Halton	6.46	2.77	0.38
Halton - scrambled	2.56	1.1	0.21
Sobol	4.58	1.65	0.19
Sobol - scrambled	2.43	1.07	0.19
LHS	2.51	1.38	0.48
Random	3.48	1.62	0.73

II. COMPARISON OF SAMPLING TECHNIQUE

In this work, we consider four different sampling techniques: two based on quasi-random sequences using Halton and Sobol sequences, the LHS technique and the classical purely random sampling method with uniform probability density function. To evaluate the performances of each technique, we rely on visual confirmation and the discrepancy as an objective figure of merit, i.e., a quantity used to describe how well the samples are geometrically equally separated (geometric uniformity) in the parameter space. There are several mathematical definitions of discrepancy [12]–[14], and in this paper, we chose the quadratic discrepancy as defined in [13].

Each approach is used to generate samples in the 6-dimensional unity hypercube $[0,1)^6$, since 6 parameters will be considered in the SFM for VCSELs in Section III. The generated samples will then be scaled to fit the required physical range for each parameter. In the results we show in this section, we consider samples in the 6-dimensional unity hypercube (without rescaling) for three different sample sizes: 50, 100 and 300 samples.
In the case of Halton and Sobol sequences, scrambling techniques can be used to reduce correlation effects and improve the quality of the sequences [15], [16]. Fig. 1 shows that patterns (correlation effects) appear for both Halton and Sobol quasi-random sequences when the sample size is small (50 or 100 points). As shown in Fig. 1(a), the shape of the pattern prevent a good coverage of the whole space and might therefore be detrimental for parameter space exploration. A common solution thus consists in scrambling the generated sequences to reduce this effect. Fig. 1(b) shows the results after scrambling. In Table I, we present the estimated discrepancy value for the different sampling schemes and number of samples, which confirms that scrambling has a beneficial impact especially for smaller sample sizes. Otherwise, the discrepancy clearly shows that quasi-random sequences with or without scrambling outperform the other schemes considered in this work.

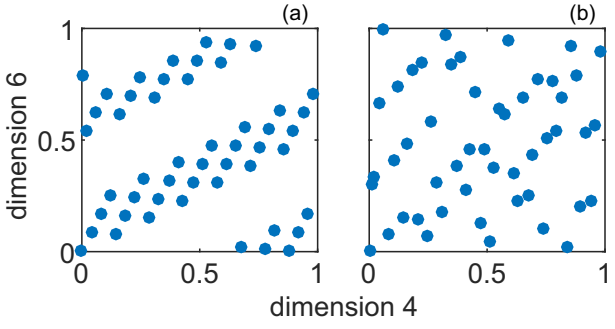

Fig. 1. Example of patterns (correlation effects) appearing in the distribution of samples generated by a 50 samples Halton sequence. (a) shows the correlation effect, and (b) shows the distribution after scrambling.

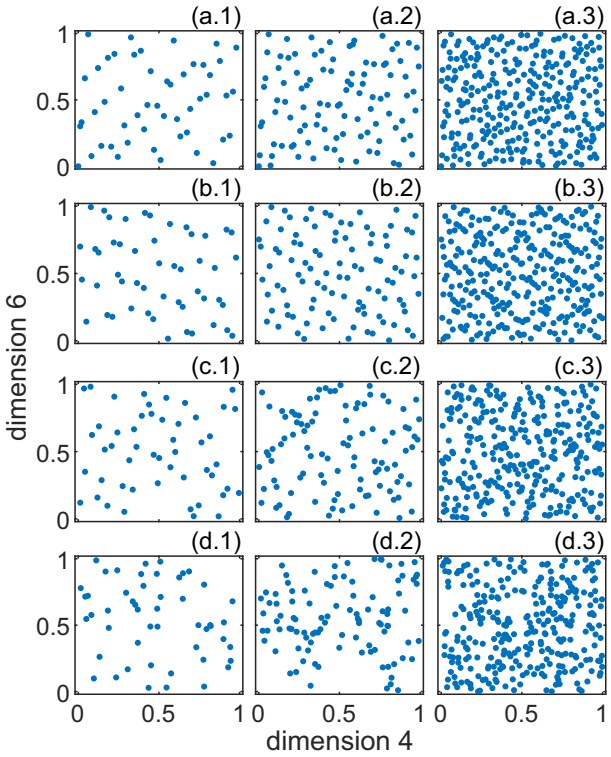

Fig. 2. Example of the evolution of sample distribution for the different sampling techniques. Each line correspond to a sampling technique: (a) Halton - scrambled, (b) Sobol - scrambled, (c) LHS, and (d) MC, and the corresponding sample distribution is shown for an increasing number of samples from left to right: (1) 50, (2) 100 and (3) 300 samples.

Finally, we compare the sample distribution for a representative dimension pair as displayed in Fig. 2. Of course this only gives a brief overview of the results, but it was not possible to plot all possible combinations for each sampling methods due to the limited amount of space available. Yet, for the sake of completeness, we made it available in [17]. Visually, we confirm previous observations: overall, Halton, Sobol and LHS provide well-distributed samples, with a significantly better distribution than a purely random approach. Although no pattern is observed even for a small number of samples, LHS has the significant drawback that the samples cannot be generated incrementally, unlike Halton and Sobol techniques, and as such requires a full re-computation to increase the sample size. Overall, Halton and Sobol sequences appear to be the most suitable advanced sampling techniques to generate 6-D samples for the exploration of the VCSEL model parameter space.

III. Spin-Flip Model for VCSELs

To investigate the polarization dynamics of VCSELs, we use the well-known SFM model [10], [11] which takes into account the competition between polarization modes and accurately reproduces the chaotic dynamics that has been observed experimentally [7]. Since only the phase difference between the two polarization modes plays a role on the system dynamics, we use the phase-amplitude decomposition proposed in [18]:

$$\frac{dR_+}{dt} = \kappa(N+n-1)R_+ - (\gamma_a cos(\Phi) + \gamma_p sin(\Phi))R_- \quad (1)$$

$$\frac{dR_-}{dt} = \kappa(N-n-1)R_- - (\gamma_a cos(\Phi) - \gamma_p sin(\Phi))R_+ \quad (2)$$

$$\frac{d\Phi}{dt} = 2\kappa\alpha n - \left(\frac{R_-}{R_+} - \frac{R_+}{R_-}\right)\gamma_p cos(\Phi) + \left(\frac{R_+}{R_-} + \frac{R_+}{R_-}\right)\gamma_a sin(\Phi) \quad (3)$$

$$\frac{dN}{dt} = -\gamma\left(-\mu + (N+n)R_+^2 + (N-n)R_-^2\right) \quad (4)$$

$$\frac{dn}{dt} = -\gamma_s n - \gamma\left((N+n)R_+^2 - (N-n)R_-^2\right) \quad (5)$$

with $R_\pm$ the amplitude of the right and left circular polarizations, Φ the phase difference between them, N the total carrier population and n the carrier population difference between the two carrier reservoirs for each circular polarization [10]. The parameters are as follows: κ and γ are the field and carrier decay rates respectively, γ_s is the spin flip relaxation rate, α is the linewidth enhancement factor, γ_p and γ_a are the phase and amplitude anisotropies respectively. For simplicity, no misalignment between amplitude and phase anisotropies is considered [19], [20].

As previously discussed, we explore the 6-D parameter space composed of the parameters discussed above. Fixing the value of γ in the model is equivalent to normalizing the SFM equations in time with respect to the carrier lifetime $1/\gamma$. We therefore fix $\gamma = 1\,ns^{-1}$ and do not consider this parameter further in this work. The variation range for the remaining 6 parameters have been defined taking into account experimental estimates in [21]–[23] and the references therein:

- The α-factor is typically around 3 for semiconductor lasers. For completeness, we consider $\alpha \in [1,\ 5]$.
- we consider injection currents up to 10 times the laser threshold i.e. $\mu \in [1,\ 10]$, which is, in practice, already a very high level that might be close to the damage threshold of the device
- The birefringence is typically of the order of a few tens of GHz, but values beyond 100 GHz have also been reached using strain techniques [24], [25]. To include all these aspects, we use $\gamma_p \in [0,\ 100]\,ns^{-1}$
- Amplitude anisotropies have typically been reported around a few ns^{-1}. For completeness, we consider both positive and negative values - which changes the steady-state that is stable at threshold [26] - and take $\gamma_a \in [-5,\ 5]\,ns^{-1}$
- For the spin-flip relaxation rate, values between a few tens up to a few thousands of ns^{-1} have been reported. Thus, we use here $\gamma_s \in [50,\ 2000]\,ns^{-1}$.
- The field decay rate is typically on the order of a few hundreds ns^{-1}, i.e. a photon lifetime of a few ps, and we take here $\kappa \in [200,\ 2000]\,ns^{-1}$. It should be noted however that for long-wavelength VCSELs significantly smaller field decay rate, of the other of tens of ns^{-1}, have been observed [23].

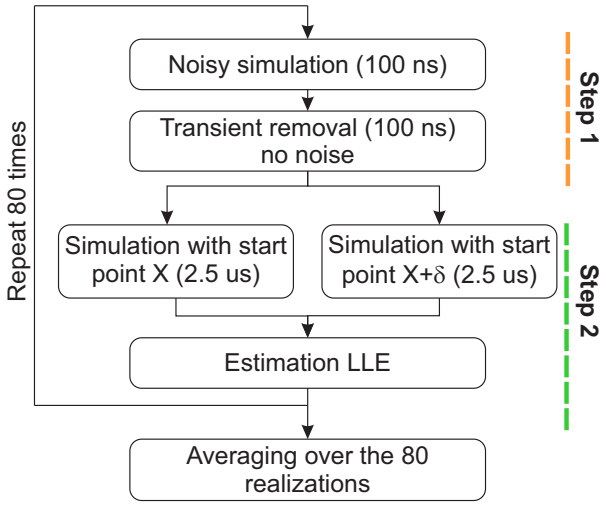

Fig. 3. Schematic of the method used to compute the Largest Lyapunov Exponent for each set of parameters based on Wolf's algorithm [27].

To identify whether the system exhibits chaotic dynamics or not for a given set of parameters, we compute the Largest Lyapunov Exponent (LLE) of the dynamics obtained for each sample using Wolf's algorithm [27]. The central idea here is to simulate two identical systems using slightly different initial conditions. Comparing the dynamical evolution of these two systems, i.e. the convergence or divergence of the two systems' trajectories in the phase space, provides a direct estimation of the LLE. It is however important to remark that the Largest Lyapunov Exponent is a time-averaged value for a given dynamical behaviour. The finite-time Lyapunov Exponents, i.e. Lyapunov Exponents computed on a short time-scale, can experience large variations and therefore extremely long simulations are required for the time-averaged value to converge, i.e. to obtain a reliable estimation of the LLE. Hence, in this context, it appears to be more efficient to perform shorter simulations but average the estimated LLE over several realizations with different initial conditions. To do so, we use a two step process as schematically displayed in Fig. 3:

- Step 1: we use noisy simulations, including a complex stochastic term modelling spontaneous emission noise for the amplitude and phase for each electrical field as done in [28], to randomly select new starting points.
- Step 2: we apply the so-called Wolf's algorithm with the starting points obtained at step 1. We simulate twice the same system - with an identical set of parameters - but in one instance we add a small random shift to the initial condition obtained in Step 1. We then evaluate the divergence of the two trajectories to estimate the Largest Lyapunov Exponent.

We follow this process 80 times and take the average LLE obtained over all realizations. This approach typically gives

an accuracy of $\pm 0.01\, ns^{-1}$ for the LLE. Nevertheless, some sets of parameter values gave atypical non-chaotic behaviour for which the estimated LLE was finite and clearly positive. To avoid these false positives, we set a threshold at $5\, ns^{-1}$ for the LLE instead of 0.

Finally, it should be noted that the goal of the noisy simulation at Step 1 is also to dismiss cases for which chaotic attractors coexist with a stable steady-state as described in [28]. Although these are expected to be relatively rare, such occurrence cannot be simply neglected. In [28], starting from the chaotic attractor, the system typically reached the stable steady-state within a few ns, to be compared with the 100 ns simulation horizon that we use here. If, despite the noisy simulation, the system remain on the chaotic attractor we can obviously conclude that the chaos is stable enough to justify its inclusion in our analysis. At the limit, i.e. when the system sometimes remain on the chaotic attractor and sometimes reaches the stable steady-state, it is clear that the estimated LLE value would be in itself meaningless. However, the coexistence of the two dynamical behaviour would justify its classification in both chaotic and non-chaotic groups. Either way, these points can be expected to be outliers but would not invalidate the interpretation of the data. Although further refinements of our classification technique might be needed for future more detailed analysis, the current approach seem to be sufficient at this stage and provide significant insight as presented below.

IV. Insight on chaotic VCSEL behavior

Using the sampled values of the parameters based on the advanced sampling techniques previously discussed, we compute the Largest Lyapunov Exponent (LLE) at each multidimensional sample in the parameter space and we can thus easily identify two groups: parameter values for which chaotic dynamic is observed and the others. In the following, considering the discrepancy figure of merit and results of the previous section, we will use the 300 values of parameters generated using the Sobol sequence (without additional scrambling). It has the best geometrical distribution in the parameter space and 14 samples have been identified as leading to chaotic dynamics. The outcome of other sampling schemes can be found in [17]. Because, all 6 dimensions of the parameter space are being explored simultaneously, we obtain a general overview of the impact of each parameter on the chaotic behaviour. We show below that this allows us to identify two general conditions which needs to be fulfilled in order to obtain polarization chaos dynamics.

Obviously, the representation of the data over 6 dimensions is a challenge, and a straigthforward way remains the so-called scatter plots as shown in Fig. 4. The 6-D sets of parameters values are projected on 2-D planes, and the sets for which chaos is obtained are identified by an orange square. For simplicity and because κ and γ_a show less impact on the chaotic dynamics, only 4 out of the 15 possible 2-D plane projections are shown. In Fig. 4, the most striking feature is probably that no chaos is observed for $\gamma_s > 500\, ns^{-1}$ (see the two panels on the right side). Chaos can be more easily

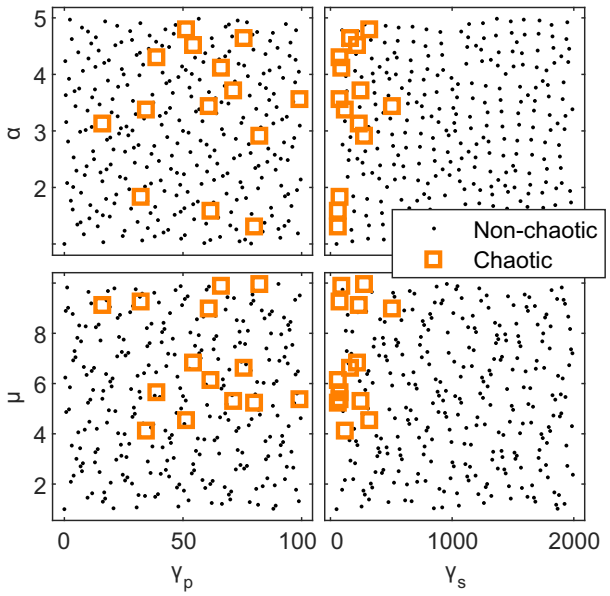

Fig. 4. 2D scatter plots of the generated parameter samples. Values leading to chaotic behaviour are identified as orange squares, while those for which no chaos is obtained are represented by black dots. On the horizontal axis, we show γ_p on the left and γ_s on the right. On the vertical axis, α is at the top while μ is at the bottom.

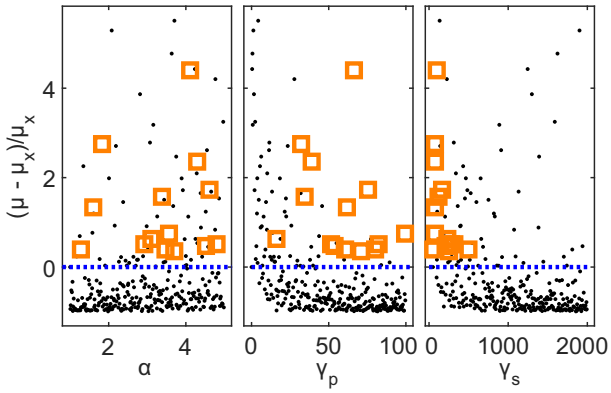

Fig. 5. 2-D scatter plots with vertical axis showing $\frac{\mu-\mu_x}{\mu_x}$. As in Fig. 4, chaotic samples are identified as an orange square, while the others are represented by a black dot. The blue horizontal dotted line gives the limit of $\mu = \mu_x$.

observed for lower values of γ_s. Second, even though it could be expected, more chaotic samples are observed for larger values of α.

Previous reports highlighted that the scenario towards deterministic polarization dynamics always follow the same steps [11], [26]: 1) a pitchfork bifurcation destabilizes the linear polarization stable at threshold and creates two elliptically polarized states, 2) Hopf bifurcations destabilize these two states, and trigger oscillations, 3) a cascade of period doubling bifurcation pushes the system towards chaos. Determining the injection current at which the Hopf bifurcation and following period doubling bifurcations can be achieved using continuation techniques, but doing so systematically for all 300 samples would be quite time-consuming. Here, as a first approximation, we use the current value at which the pitchfork bifurcation

occurs for $\gamma_a = 0$, which can be calculated analytically [11]:

$$\mu_x = 1 + \frac{1}{\gamma}\frac{\gamma_s\gamma_p}{\kappa\alpha - \gamma_p} \tag{6}$$

For $\gamma_a \neq 0$, the expression becomes much more complicated [29], yet (6) remains an excellent approximation in practice. Thus, μ_x would therefore be a lower bound of the region of chaotic dynamics in terms of injection current. To confirm it, we again use scatter plots shown in Fig. 5 but this time with $(\mu - \mu_x)/\mu_x$ instead of μ. As expected, μ_x indeed seems to be a lower bound for the chaotic regions as no chaotic sample is observed for $\mu < \mu_x$, i.e. below the blue dotted line. Although our 300 samples are well distributed across the parameter space, only a fraction of these samples meets the condition $\mu > \mu_x$: only 74 out of 300 samples. This therefore suggests that only a small part of the 6D parameter space would be of interest to generate polarization chaos. Considering the expression of μ_x in (6), large values of γ_p and γ_s will lead to higher values of the lower bound. As a result, a balance between the two parameters are needed to obtain chaos within a realistic range of injection currents which is exactly what we observe: chaos appears for low values of γ_s and relatively large values of γ_p simultaneously. Here, it is worth reminding the reader that we only consider currents up to 10 times the laser threshold, which is already quite large in practice. Similarly, larger values of α and κ will help decrease the value of μ_x hence favouring the emergence of chaotic dynamics. Last, we see in the middle panel of Fig. 5 that non chaotic samples with $\mu > \mu_x$ mostly appear for lower values of γ_p. Besides the low-value of μ_x, this can also be explained by a comparatively short region of chaotic dynamics for small birefringence values [26], but also possibly by the coexistence of a chaotic attractor and a steady-state as discussed in [28].

Similarly, we can try to find an upper bound of the chaotic region with respect to the injection current. After the complex polarization dynamics, when increasing the injection current, the laser is expected to settle on a steady-state with a linear polarization, orthogonal to the polarization at threshold. Typically this steady-state becomes stable via a Hopf bifurcation. Again, the current value at which the bifurcation occurs can be obtained analytically for $\gamma_a = 0$ [11]:

$$\mu_y = 1 - \gamma_s + \frac{2\alpha\gamma_p}{\gamma} \tag{7}$$

This expression is hardly valid for $\gamma_a \neq 0$ [11], and the bifurcation itself is not always an upper limit for the chaotic region as seen for $\gamma_p = 4\,ns^{-1}$ in [26]. Nevertheless, the corresponding scatter plots using $\mu - \mu_y$ in the vertical axis give an interesting output. Thus, apart from two clear outliers, all other samples are below the $\mu = \mu_y$ limit. $|\mu_y|$ appears to be quite large compared to μ, hence the system's position in the planes of Fig. 6 will be mostly determined by the value of $-\mu_y$. Positive values of μ_y ($\mu - \mu_y < 0$) seem to overall favour the emergence of chaotic dynamics. From the analytical expression (7), we can quickly reach the following approximated condition

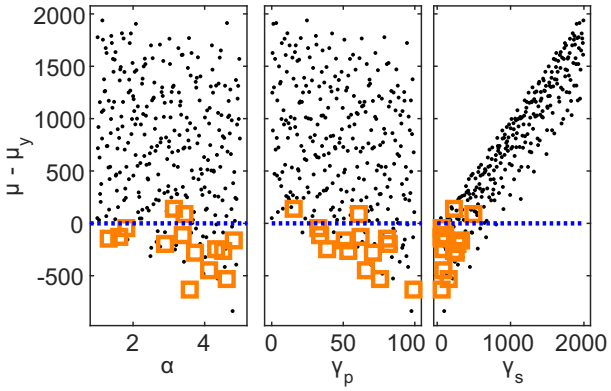

Fig. 6. 2-D scatter plots with vertical axis showing $\mu - \mu_y$. As in Fig. 4, chaotic samples are identified as an orange square, while the others are represented by a black dot. The blue horizontal dotted line gives the limit of $\mu = \mu_y$.

$(\gamma_s - 1)\gamma > 2\alpha\gamma_p$ that should be fulfilled to obtain $\mu_y < 0$. Interestingly this expression characterizes again the balance between γ_s and γ_p. Of course, the existence of outliers highlights the imperfection of this condition, but, even though further confirmation would be required, the data at hands suggest that this condition is in practice a good approximation.

From the perspective of VCSEL dynamics, we highlight that chaotic dynamics is relatively rare, from a statistical point of view with an occurrence of the order of only 5% in the range of parameters considered here. However, we are able to come up with a few general conditions that need to be fulfilled in order to obtain chaos in a free-running VCSEL. At first glance, γ_s seems to be the limiting parameter for which extremely small values are required. However, going a bit further, the injection current is in fact the parameter which seems to be the most constrained. First, in VCSELs, the maximal value of the injection current is limited to about 5 to 10 times the current threshold to avoid damaging the device [30], [31]. Second, the polarization mode at threshold needs to be unstable, i.e. $\mu > \mu_x$. Third, the system needs to remain in the chaotic region for which the upper boundary can be approximated by $\mu < \mu_y$. Both μ_x and μ_y are strongly dependent on the balance between two main parameters: the spin-flip rate γ_s and the birefringence γ_p, hence motivating more in-depth investigation focusing on these two parameters. Even though the spin-flip rate can be relatively large (in the order of $1000\,ns^{-1}$ [23]), the possibility to efficiently tune the birefringence, e.g. through strain techniques [24], [25], [32], suggest that polarization chaos could potentially be achieved in any VCSEL devices.

V. Conclusion

We have shown that it is possible to gain a significant and general insight on the complex behaviour of VCSELs with a reduced number of samples in the parameter space by using advanced sampling schemes, and thus a reduced amount of computing time. Here, only 300 samples has been used to cover a 6-D parameter space. As a comparison reference,

3 samples per dimension in a standard tensor-product grid would already lead to 729 samples (more than twice the number of samples considered here) and this approach would be very unlikely to bring the same level of information. In fact similar discrepancy values are only obtained when millions of points are considered. On the other hand, with a purely random sampling there are no guarantees that the samples will indeed be uniformly distributed across the whole parameter space. Hence, this scheme might again require much more samples to give a sufficient coverage. Sobol and Halton sampling schemes result to better choices to explore the parameter space.

From the perspective of chaotic dynamics in VCSELs, this approach allowed us to confirm that μ_x and μ_y can be reasonably used as an approximation of the lower and upper bound of the chaotic region in terms of injection current. Moreover, we showed that the balance between the birefringence and the spin-flip rate seems to be the key to effectively achieve polarization chaos hence motivating the use of birefringence tuning techniques to potentially trigger the dynamics in commercial VCSELs [24], [25], [32]. This solution has been recently demonstrated in [9] as strain-induced polarization chaos was obtained in a commercial VCSEL. Unfortunately, in this experimental work, the birefringence and the spin-flip relaxation rate could not be measured. Yet, the reported features are coherent with the theoretical framework described here. Future work will be focused on further enhancing the discussed parameter space exploration methodology by adding a feature of adaptivity in order to refine an initial sampling distribution and add samples in an adaptive loop. This will allow focusing more samples in the regions where chaos is most likely to appear.

Finally, we should emphasize that, independently of the method used, sampling-based techniques can only provide a partial overview of the system behaviour, since only a finite number of samples is used. Thus, as it can be seen in the supplementary information [17], the different sampling schemes can uncover different regions of chaotic dynamics. Our approach aims to minimize the number of samples and maximize the insight in the system behaviour. This could represent a significant advantage for investigations of various complex systems, such as other types of semiconductor lasers subject to feedback or injection [4]–[6], nonlinear fiber-based polarization scrambler [33], fiber-lasers [34] or chaos-based reinforcement learning systems [35].

REFERENCES

[1] W.-L. Loh, "On latin hypercube sampling," *Ann. Statist.*, vol. 24, no. 5, pp. 2058–2080, 1996.

[2] I. Sobol, "On the distribution of points in a cube and the approximate evaluation of integrals," *USSR Computational Mathematics and Mathematical Physics*, vol. 7, no. 4, pp. 86 – 112, 1967.

[3] W.-S. L. T.-T. Wong and P.-A. Heng, "On the distribution of points in a cube and the approximate evaluation of integrals," *Journal of Graphics Tools*, vol. 2, no. 2, pp. 9 – 24, 1997.

[4] C. Bonatto, M. Feyereisen, S. Barland, M. Giudici, C. Masoller, J. R. R. Leite, and J. R. Tredicce, "Deterministic Optical Rogue Waves," *Physical Review Letters*, vol. 107, no. 5, p. 053901, jul 2011.

[5] J. P. Toomey and D. M. Kane, "Mapping the dynamic complexity of a semiconductor laser with optical feedback using permutation entropy," *Optics Express*, vol. 22, no. 2, p. 1713, 2014.

[6] D. O'Shea, S. Osborne, N. Blackbeard, D. Goulding, B. Kelleher, and A. Amann, "Experimental classification of dynamical regimes in optically injected lasers," *Optics Express*, vol. 22, no. 18, p. 21701, 2014.

[7] M. Virte, K. Panajotov, H. Thienpont, and M. Sciamanna, "Deterministic polarization chaos from a laser diode," *Nature Photon.*, vol. 7, no. 1, pp. 60–65, nov 2013.

[8] F. Hopfer, A. Mutig, M. Kuntz, G. Fiol, D. Bimberg, N. N. Ledentsov, V. A. Shchukin, S. S. Mikhrin, D. L. Livshits, I. L. Krestnikov, a. R. Kovsh, N. D. Zakharov, and P. Werner, "Single-mode submonolayer quantum-dot vertical-cavity surface-emitting lasers with high modulation bandwidth," *Appl. Phys. Lett.*, vol. 89, no. 14, p. 141106, 2006.

[9] T. R. Raddo, K. Panajotov, B.-H. V. Borges, and M. Virte, "Strain induced polarization chaos in a solitary VCSEL," *Scientific Reports*, vol. 7, no. 1, p. 14032, 2017. [Online]. Available: http://www.nature.com/articles/s41598-017-14436-3

[10] M. San Miguel, Q. Feng, and J. V. Moloney, "Light-polarization dynamics in surface-emitting semiconductor lasers," *Phys. Rev. A*, vol. 52, no. 2, pp. 1728–1739, 1995.

[11] J. Martin-Regalado, F. Prati, M. S. Miguel, and N. Abraham, "Polarization properties of vertical-cavity surface-emitting lasers," *IEEE J. Quantum Electron.*, vol. 33, no. 5, pp. 765–783, 1997.

[12] H. Niederreiter, *Random Number Generation and quasi-Monte Carlo Methods*. Philadelphia, PA, USA: Society for Industrial and Applied Mathematics, 1992.

[13] F. James, J. Hoogland, and R. Kleiss, "Multidimensional sampling for simulation and integration: measures, discrepancies, and quasi-random numbers," *Computer Physics Communications*, vol. 99, no. 2, pp. 180 – 220, 1997.

[14] F. J. Hickernell, "A generalized discrepancy and quadrature error bound," *Math. Comput.*, vol. 67, no. 221, pp. 299–322, Jan. 1998.

[15] R. Wyrzykowski, J. Dongarra, K. Karczewski, and W. Jerzy, *Parallel processing and applied mathematics : 8th international conference*. Berlin New York: Springer, 2010.

[16] L. Plaskota and H. Wozniakowski, *Monte carlo and quasi-monte carlo methods*. Berlin New York: Springer, 2012.

[17] M. Virte and F. Ferranti. (2017) Chaos in solitary vcsels: Exploring parameter space with advanced sampling (supplementary information). [Online]. Available: https://dx.doi.org/10.6084/m9.figshare.5242213

[18] T. Erneux, J. Danckaert, K. Panajotov, and I. Veretennicoff, "Two-variable reduction of the San Miguel-Feng-Moloney model for vertical-cavity surface-emitting lasers," *Phys. Rev. A*, vol. 59, no. 6, p. 4660, jun 1999.

[19] M. Travagnin, "Linear anisotropies and polarization properties of vertical-cavity surface-emitting semiconductor lasers," *Phys. Rev. A*, vol. 56, no. 5, p. 4094, nov 1997.

[20] M. Virte, E. Mirisola, M. Sciamanna, and K. Panajotov, "Asymmetric dwell-time statistics of polarization chaos from free-running VCSEL," *Opt. Lett.*, vol. 40, no. 8, pp. 1865–1868, 2015.

[21] M. P. van Exter, M. B. Willemsen, and J. P. Woerdman, "Polarization fluctuations in vertical-cavity semiconductor lasers," *Phys. Rev. A*, vol. 58, no. 5, p. 4191, nov 1998. [Online]. Available: http://link.aps.org/doi/10.1103/PhysRevA.58.4191

[22] M. Sondermann, M. Weinkath, and T. Ackemann, "Polarization Switching to the Gain Disfavored Mode in Vertical-Cavity Surface-Emitting Lasers," *IEEE J. Quantum Electron.*, vol. 40, no. 2, p. 97, 2004.

[23] P. Pérez, A. Valle, and L. Pesquera, "Polarization-resolved characterization of long-wavelength vertical-cavity surface-emitting laser parameters," *J. Opt. Soc. Am. B*, vol. 31, no. 11, pp. 2574–2580, Nov 2014. [Online]. Available: http://josab.osa.org/abstract.cfm?URI=josab-31-11-2574

[24] T. Pusch, M. Lindemann, N. C. Gerhardt, and M. R. Hofmann, "Vertical-cavity surface-emitting lasers with birefringence splitting above 250 GHz," *Electron. Lett.*, vol. 51, no. 20, pp. 1600–1602, 2015.

[25] M. Lindemann, T. Pusch, R. Michalzik, N. C. Gerhardt, and M. R. Hofmann, "Frequency tuning of polarization oscillations: Toward high-speed spin-lasers," *Applied Physics Letters*, vol. 108, no. 4, p. 042404, 2016.

[26] M. Virte, K. Panajotov, and M. Sciamanna, "Bifurcation to nonlinear polarization dynamics and chaos in vertical-cavity surface-emitting lasers," *Phys. Rev. A*, vol. 87, no. 1, p. 013834, jan 2013.

[27] A. Wolf, J. B. Swift, H. L. Swinney, and J. A. Vastano, "Determining Lyapunov exponents from a time series," *Physica D*, vol. 16, no. 3, p. 285, jul 1985.

[28] M. Virte, "Noise induced stabilization of chaotic free-running laser diode," *Chaos*, vol. 26, no. 5, p. 053108, 2016.
[29] F. Prati, P. Caccia, M. Bache, and F. Castelli, "Analysis of elliptically polarized states in vertical-cavity-surface-emitting lasers," *Phys. Rev. A*, vol. 69, no. 3, p. 033810, mar 2004.
[30] Philips Photonics N.V. (2017) High-speed vcsel and photodiodes, specifications. [Online]. Available: http://www.photonics.philips.com/products/high-speed-vcsel-and-pd
[31] Ray Can. (2017) Vcsel products specifications. [Online]. Available: http://www.raycan.com/product.html
[32] A. K. Jansen van Doorn, M. P. van Exter, and J. P. Woerdman, "Tailoring the birefringence in a vertical-cavity semiconductor laser," *Appl. Phys. Lett.*, vol. 69, no. 24, p. 3635, 1996.
[33] M. Guasoni, P. Y. Bony, M. Gilles, A. Picozzi, and J. Fatome, "Fast and Chaotic Fiber-Based Nonlinear Polarization Scrambler," *IEEE Journal on Selected Topics in Quantum Electronics*, vol. 22, no. 2, pp. 1–13, 2016.
[34] C. Lecaplain, P. Grelu, and S. Wabnitz, "Dynamics of the transition from polarization disorder to antiphase polarization domains in vector fiber lasers," *Physical Review A - Atomic, Molecular, and Optical Physics*, vol. 89, no. 6, pp. 25–28, 2014.
[35] M. Naruse, Y. Terashima, A. Uchida, and S. J. Kim, "Ultrafast photonic reinforcement learning based on laser chaos," *Scientific Reports*, vol. 7, no. 1, pp. 1–29, 2017.

Martin Virte received the master in engineering with a major in Photonics from the French Grande Ecole Supélec (now CentraleSupélec, Université de Paris-Saclay, France) and the M.Sc. in Physics from Supélec and the Université de Lorraine both in 2011. Later, in the frame of a joint PhD program, he simultaneously obtained the PhD degree in Photonics from Supélec and in engineering from the Vrije Universiteit Brussels, Brussels, Belgium in 2014. Since then, Martin has been a post-doctoral researcher at Brussels Photonics (B-PHOT), Vrije Universiteit Brussel, Belgium. In 2015, he received a three-year fellowship from the Research Foundation Flanders (FWO) to pursue his research in Belgium.
Martin received the Graduate Student Fellowship Award from the IEEE Photonics Society in 2014 in recognition of his PhD work. The same year, he received the prix de la publication from the Foundation Supélec awarded to the Supélec PhD graduate with the best record in terms of publications. So far Martin authored and co-authored more than 13 papers in international refereed journals and several contributions in national and international conferences. His research is currently focusing on laser dynamics, more competition, optical chaos and their applications in sensing and communication. In addition, he acts as a reviewer for several international journals including journal of lightwave technology, chaos, applied physics letters and others. He is a member of SPIE, the IEEE Photonics Society and OSA.

Francesco Ferranti (M'10-SM'17) received the Ph.D. degree in electrical engineering from Ghent University, Ghent, Belgium, in 2011. He is currently an Associate Professor at the Microwave Department at Institut Mines-Télécom (IMT), Brest, France. He has been awarded the Anile-ECMI Prize for Mathematics in Industry 2012 and the Electromagnetic Compatibility Society President's Memorial Award 2012.

He has authored and co-authored 51 papers in international peer-reviewed journals, 46 papers in international peer-reviewed conferences and 2 books chapters. He has given invited lectures and chaired several sessions at international conferences. He serves as a regular reviewer for several international journals. He is a Senior IEEE member.

His research interests include parameterized modeling and model order reduction, sampling techniques, design space exploration, uncertainty quantification, optimization, applied electromagnetics, behavioral modeling, microwave design and characterization, and multiphysics modeling.